Available online at www.sciencedirect.com

ScienceDirect

www.elsevier.com/locate/jes

JES JOURNAL OF ENVIRONMENTAL SCIENCES

www.jesc.ac.cn

Photodegradation of Orange II using waste paper sludge-derived heterogeneous catalyst in the presence of oxalate under ultraviolet light emitting diode irradiation

*Guoqiang Zhou, Jinyi Guo, Guowang Zhou, Xiankai Wan, Huixiang Shi**

Department of Environmental Engineering, Zhejiang University, Yuhangtang Road 866, Hangzhou, Zhejiang 310058, China

ARTICLE INFO

Article history:
Received 10 September 2015
Revised 27 November 2015
Accepted 1 December 2015
Available online 24 March 2016

Keywords:
Heterogeneous catalyst
Waste paper sludge
Oxalic acid
Orange II

ABSTRACT

A waste paper sludge-derived heterogeneous catalyst (WPS-Fe-350) was synthesized via a facile method and successfully applied for the degradation of Orange II in the presence of oxalic acid under the illumination of ultraviolet light emitting diode (UV-LED) Powder X-ray diffraction, Fourier-transform infrared spectroscopy, scanning electronic microscopy and N_2 sorption isotherm analysis indicated the formation of α-Fe_2O_3 in the mesoporous nanocomposite. The degradation test showed that WPS-Fe-350 exhibited rapid Orange II (OII) degradation and mineralization in the presence of oxalic acid under the illumination of UV-LED. The effects of pH, oxalic acid concentration and dosage of the catalyst on the degradation of OII were evaluated, respectively. Under the optimal conditions (1 g/L catalyst dosage, 2 mmol/L oxalic acid and pH 3.0), the degradation percentage for a solution containing 30 mg/L OII reached 83.4% under illumination by UV-LED for 80 min. Moreover, five cyclic tests for OII degradation suggested that WPS-Fe-350 exhibited excellent stability of catalytic activity. Hence, this study provides an alternative environmentally friendly way to reuse waste paper sludge and an effective and economically viable method for degradation of azo dyes and other refractory organic pollutants in water.

Introduction

The photo-Fenton process, as one of the most popular advanced oxidation processes (AOPs), is extensively applied in the treatment of industrial wastewaters (Oller et al., 2011). The photo-Fenton system mainly involves the formation of strongly oxidizing hydroxyl radicals (•OH), which can completely mineralize most organic compounds due to their high oxidation potential (E^0 = +2.8 V *versus* normal hydrogen electrode) (Haag and David Yao, 1992). Recently, photo-Fenton and photo-Fenton-like reactions have been widely employed as effective methods to degrade azo dyes (Chen et al., 2013; Guo et al., 2014, 2015; Liu et al., 2012). In these reactions, H_2O_2 is necessary to initiate the process, because H_2O_2 is the only source of •OH (Kremer, 1999; Pera-Titus et al., 2004). However, H_2O_2 is a very reactive chemical reagent with high oxidizing power and does not survive for long under normal conditions. Thus, the direct use of reactive H_2O_2 is inconvenient for practical industrial applications.

Polycarboxylic acids and iron oxides are capable of forming a photochemical system to initiate a photo-Fenton-like reaction generating •OH without the addition of H_2O_2 (Lei et al., 2006). It is notable that Fe(III)-carboxylate complex photochemical systems can achieve higher quantum efficiency than that of

* *Corresponding author*. E-mail: 11214033@zju.edu.cn (Huixiang Shi).

http://dx.doi.org/10.1016/j.jes.2015.11.030
1001-0742/

the photo-Fenton process or photocatalytic reaction with Fe(III) alone (Faust and Zepp, 1993; Li et al., 2007; Siffert and Sulzberger, 1991; Zuo and Deng, 1997). The photoexcitation of Fe(III)-carboxylate complexes can form Fe(II) and carboxylate radicals via a ligand-to-metal charge transfer (LMCT) mechanism, which has been previously elucidated in detail (Balmer and Sulzberger, 1999; Zuo and Deng, 1997).

It is well known that the usage of ultraviolet (UV) light sources is one of the major drawbacks limiting the commercialization of photocatalytic technologies. Low-pressure mercury vapor lights are typically employed as the UV source in conventional photocatalytic reactions, and have some drawbacks, such as containing highly toxic mercury, being relatively energy intensive and having short life spans. However, ultraviolet light emitting diode (UV-LED) can substitute for mercury lamps in photocatalytic process. UV-LED does not contain toxic mercury and have the advantages of longer life spans and lower energy consumption, allowing flexibility in engineering application (Hossaini et al., 2014). UV-LED has been successfully applied in photocatalysis processes for the degradation of several xenobiotics, including formaldehyde (Shie et al., 2008), bisphenol (Wang and Lim, 2010), and chlorophenol (Yu et al., 2013) in contaminated wastewater. However, little has been reported about the application of UV-LED as UV light-sources in Fe(III)-carboxylate complexes involved in photo-Fenton-like processes so far.

Recently, various kinds of supports such as mesoporous activated carbon (Karthikeyan et al., 2011), nanoporous activated carbon, activated carbon fibers (Karthikeyan et al., 2014), zeolites (Fukuchi et al., 2014), resins (Shu et al., 2010), and hydrogel (Wang et al., 2014) have been used to prepare heterogeneous photo-Fenton or photo-Fenton-like catalysts. However, these efficient catalysts have challenges in terms of high cost of production and technical complexity, to some extent, which limit their full-scale practical application. Thus, a major issue researchers confront is the development of a novel and highly active catalyst with a facile and low-cost synthesis process, which is suitable for extensive engineering application. On the other hand, an increasing amount of sludge is generated as a byproduct of the paper wastewater treatment process, which contains 20% or more solids, with 45%–55% moisture, which would cause serious environmental problems in the event of inappropriate management and disposal (Hamzeh et al., 2011). More recently, waste paper sludge has been used by converting it into mesoporous adsorbents to remove organic pollutants from water or reclaimed as an industrial raw material (Calisto et al., 2014; Devi and Saroha, 2014; Hamzeh et al., 2011). These methods are among the most feasible and environmentally friendly ways to make use of waste paper sludge. It is anticipated that waste paper sludge can be converted into a heterogeneous photo-Fenton-like catalyst of high catalytic activity.

The present study aimed to evaluate the potential of an as-synthesized catalyst (WPS-Fe-350) to degrade Orange II (OII) (as a model pollutant) in the presence of oxalic acid by using UV-LEDs as the activation source. Several significant factors such as the catalyst dosage, oxalic acid concentration and pH were investigated to optimize the reaction conditions and gain a clear understanding of this photochemical reaction. To the best of our knowledge, this is the first attempt to use a waste paper sludge-derived catalyst for effective degradation of OII in the presence of oxalic acid under illumination of UV-LEDs.

1. Experimental

1.1. Materials

The hydrous waste paper sludge used as raw material for the synthesis of catalyst in this study was sampled from a paper mill effluent treatment plant located in Zhejiang, China, with a designed capacity of 20,000 m^3/day. The moisture content of the wet sludge was 89.7% ± 0.3%. The sludge was stored at 4°C before use. Ferrous sulfate ($FeSO_4 \cdot 4H_2O$) and oxalic acid ($H_2C_2O_4$) were purchased from Aldrich Co. Orange II ($C_{16}H_{11}N_2NaO_4S$, 99.9%) was acquired from Fluka Co. All reagents were analytical grade unless otherwise stated. All of the solutions were prepared with water from a water purification system (Merck Millipore Co., Shanghai, China). Diluted solutions of sodium hydroxide or hydrochloric acid were employed for pH adjustment.

1.2. Preparation of catalyst

The dewatered waste paper sludge sample was dried at 105°C for 24 hr, and ground and sieved to a uniform size of <0.1 mm. Then the sample was heated to 350°C in a muffle furnace in air for 2 hr to obtain the material designated as WPS-350. The waste paper sludge-derived catalyst was prepared following the procedure below: a 10 g ground and sieved sample was impregnated in a 100 mL of 1 mol/L $FeSO_4$ solution for 24 hr at room temperature. After the supernatant liquid was completely removed, the sample was dried at 105°C for another 24 hr. Subsequently, the sample was heated to 350°C in a muffle furnace in air for 2 hr to obtain the material designated as WPS-Fe-350. Finally, the catalyst was washed three times with 95% alcohol and another three times with distilled water to remove anions and organic impurities. The waste paper sludge-derived Fe-loaded nanocomposite was designated as WPS-Fe-350 and used for characterization and degradation experiments.

1.3. Characterization of catalyst

The crystal phase was determined by X-ray diffraction (XRD, Ultima IV, Rigaku Co., Japan) with monochromatic Cu Kα radiation (45 kV, 50 mA). The functional groups were detected by Fourier transform infrared (FT-IR) spectroscopy (Nexus, Thermo Nicolet Lt., USA) using the potassium bromide (KBr) pellet method. The surface morphology was analyzed by scanning electron microscopy (SEM, FEI Co., The Netherlands). The specific surface area (S_{BET}), micropore surface and total pore volume were measured by the Brunauer–Emmett–Teller (BET) method (ASIC-2, PE Co., USA). The bulk chemical composition was analyzed via an energy dispersive X-ray detector (EDX) attached to the SEM.

1.4. Experimental procedures

The degradation experiments were conducted in a glass photoreactor, which has an internal diameter of 12 cm and a

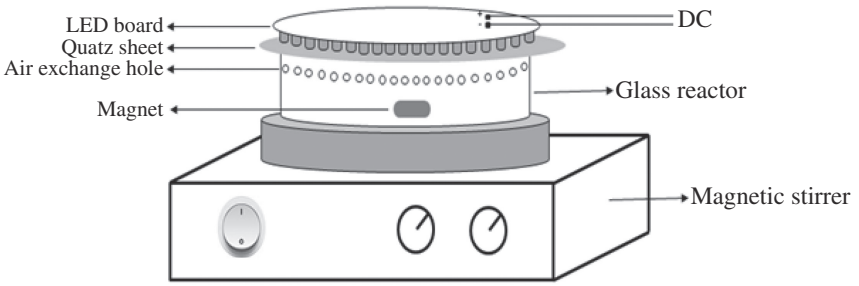

Fig. 1 – Schematic diagram of the experimental setup.

total volume of 150 mL. The schematic of the photoreaction setup is shown in Fig. 1. A set of 75 GaN LEDs (Semiconductor, Korea) was used as the light source, with a maximum intensity at 385 nm. The UV-LEDs were installed on round aluminum plate. A quartz filter was fixed between the UV-LEDs and the reactor. The UV-LEDs were connected in series to a direct current (DC) power system with a maximum current intensity of 20 mA. The distance from the surface of the UV-LEDs to the liquid level in the reactor was 2 cm.

In a typical experimental run, 100 mL of OII solution (100 mg/L) and a varying amount of catalyst was added into the photoreactor. The initial pH was adjusted to 3 by using 0.1 mol/L HCl or NaOH for consistency. After mixing for 30 min to achieve equilibrium for catalyst dissolution and iron-ligand chelation, the reaction was initiated by switching on the light source and the suspension was then constantly stirred at 120 r/min with a magnetic stirrer during the reaction process. Sample aliquots of 1 mL of the suspension were withdrawn at intervals and centrifuged at 5000 r/min for 10 min, then filtered via a Millipore filter (0.45 μm) to separate any catalyst particles. OII absorbance was measured at its maximum absorbance of 485 nm with an ultraviolet–visible (UV–Vis) spectrophotometer (UV1750, Shimadzu Co., Japan), and its concentration was determined from a calibration curve. The content of total organic carbon (TOC) was measured by a TOC analyzer (TOC-V, CPH, Shimadzu Co., Japan).

2. Results and discussion

2.1. Characterization of the catalyst

The XRD patterns of WPS-350 and WPS-Fe-350 (catalyst) are shown in Fig. 2. The diffractograms suggest that the two materials displayed similar intense diffraction peaks at 2θ of 25.4 and 29.4°, which corresponded to typical $CaSO_4$ (Anhydrite) and $CaCO_3$ (Calcite) crystalline structures respectively. Compared with WPS-350, the peaks at 2θ of 33.1, 35.6 and 40.8° of WPS-Fe-350 were in agreement with the (104), (110) and (113) reflection data in JCPDS No. 84-0306 of α-Fe_2O_3. Thus, the XRD data confirmed that α-Fe_2O_3 is the main iron oxide present in the as-synthesized catalyst WPS-Fe-350.

The FT-IR spectra of WPS-350 and WPS-Fe-350 (as-synthesized catalyst) are shown in Fig. 3. The peaks at 3451 and 1638 cm^{-1} corresponded to the O–H stretching and bending vibrations, respectively (Yuan and Dai, 2014). The peak at 2932 cm^{-1} corresponded to the stretching vibration of C–H in the CH_3 and CH_2 groups. In contrast with WPS-350, the peak at 1442 cm^{-1} became weak in the spectrum of WPS-Fe-350, which corresponded to the symmetrical deformations of CH_2 (Yuan and Dai, 2014).

The pore size distribution curves and N_2 adsorption–desorption isotherms of WPS-350 compared with WPS-Fe-350 are shown in Fig. 4a1, a2, respectively. WPS-Fe-350 (S_{BET}, 16.49 m^2/g) had a smaller specific surface area than WPS-350

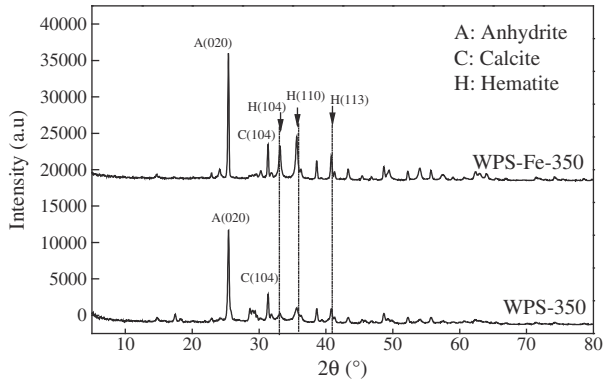

Fig. 2 – XRD pattern of waste paper sludge-derived catalyst (A represents Anhydrite, C represents Calcite, H represents hematite). WPS-Fe-350 and WPS-350 refer to Section 1.2.

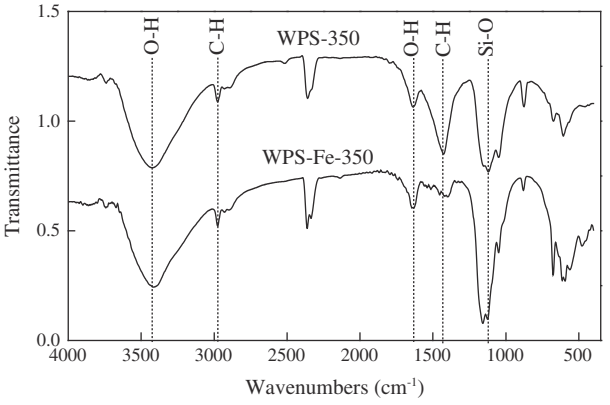

Fig. 3 – FT-IR spectra of waste paper sludge-derived catalysts.

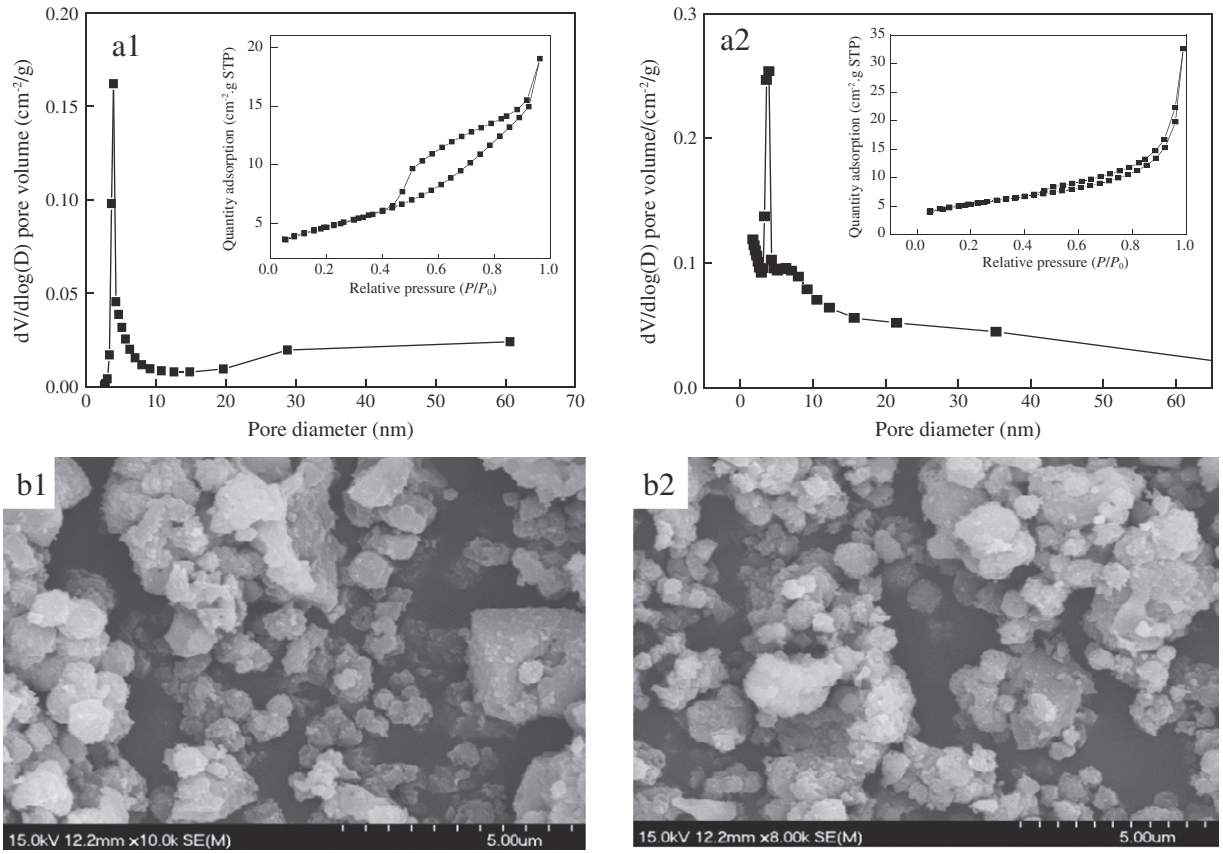

Fig. 4 – (a) Pore size distribution and (b) SEM images of (1) WPS-350 and (2) WPS-Fe-350.

(S_{BET}, 18.64 m^2/g), which may be attributed to the blocking of some pores of the catalyst by the loading of Fe and an increase in density after calcination and Fe loading. The results also proved the existence of large-pore mesopores in the range of 2–50 nm, which was favorable for the catalytic properties of WPS-Fe-350. All the isotherms were close to type IV isotherms as classified according to International Union of Pure and Applied Chemistry (IUPAC). The SEM images of WPS-350 and WPS-Fe-350 are shown in Fig. 4b1 and b2. WPS-350 and WPS-Fe-350 exhibited coarse and nonporous surfaces, which was due to the evaporation of H_2O or decomposition of organic molecules during the calcination process and can offer more adsorption sites for the catalyst.

2.2. Degradation of OII under different systems

The experimental results of OII photodegradation under different conditions are presented in Fig. 5. Without the addition of oxalic acid, when the solution mixed with OII and WPS-Fe-350 was subjected to UV-LED irradiation for 80 min, the concentration of OII was only slightly decreased, by 2.4%, which was thought to be due to adsorption rather than degradation. After the addition of oxalic acid, only 2.7% degradation of OII was reached after 80 min without illumination by UV-LEDs. A 13.5% degradation ratio was observed in the mixed solution of oxalic acid and OII without WPS-Fe-350 under illumination by UV-LEDs. The reason was due to the direct electron transfer between the photo-excited state of OII and oxalic acid ions (Wei et al., 2012). When both oxalic acid and WPS-Fe-350 together were added to the OII solution to form the photo-Fenton-like photochemical reaction under UV-LED irradiation, the degradation percentage of OII was significantly increased to 86.4% after 80 min reaction. As determined by the TOC measurement, 44.5% TOC removal was detected in 80 min, suggesting that WPS-Fe-380 showed high OII mineralization efficiency.

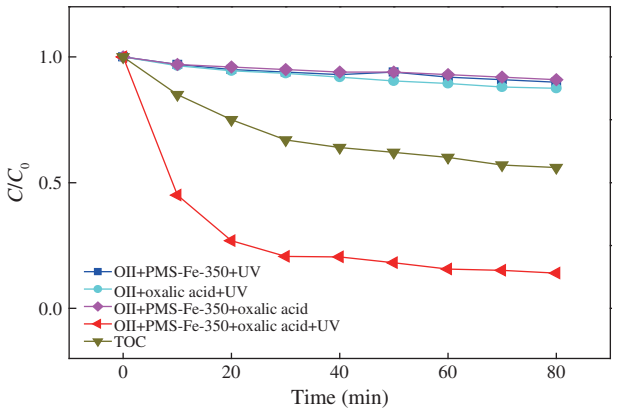

Fig. 5 – Relative concentration profiles of OII and TOC during typical degradation processes under various systems.

2.3. Effect of pH

To investigate the influence of pH on the photodegradation of OII, a series of experiments was conducted at different initial pH values. As depicted by Fig. 6a, OII can be degraded with WPS-Fe-350 in the presence of oxalic acid within the pH range 2–5. The degradation percentage of OII reached a maximum (above 80%) at pH 3. When the reaction system was set at an initial pH of 3, the main Fe(III)-oxalate species on the solid catalyst surface were $[\equiv Fe^{III}(C_2O_4)_n]^{3-2n}$, which were highly photoactive (Balmer and Sulzberger, 1999). However, the degradation of OII was inhibited obviously when the system pH was outside the range 3–4. When the system pH was lower than 2, the low degradation percentage was due to the scavenging of •OH by H^+ (Liu et al., 2012). However, when the reaction system pH value was set at 4–5, $[\equiv Fe^{III}(C_2O_4)_2]^+$ was the main form of Fe(III)-oxalate complex, with low photoactivity. When the initial system pH was set at 6, the predominant Fe(III) species was Fe(III)–OH, which has little or no photoactivity. Thus, the optimal pH is 3 for this reaction system.

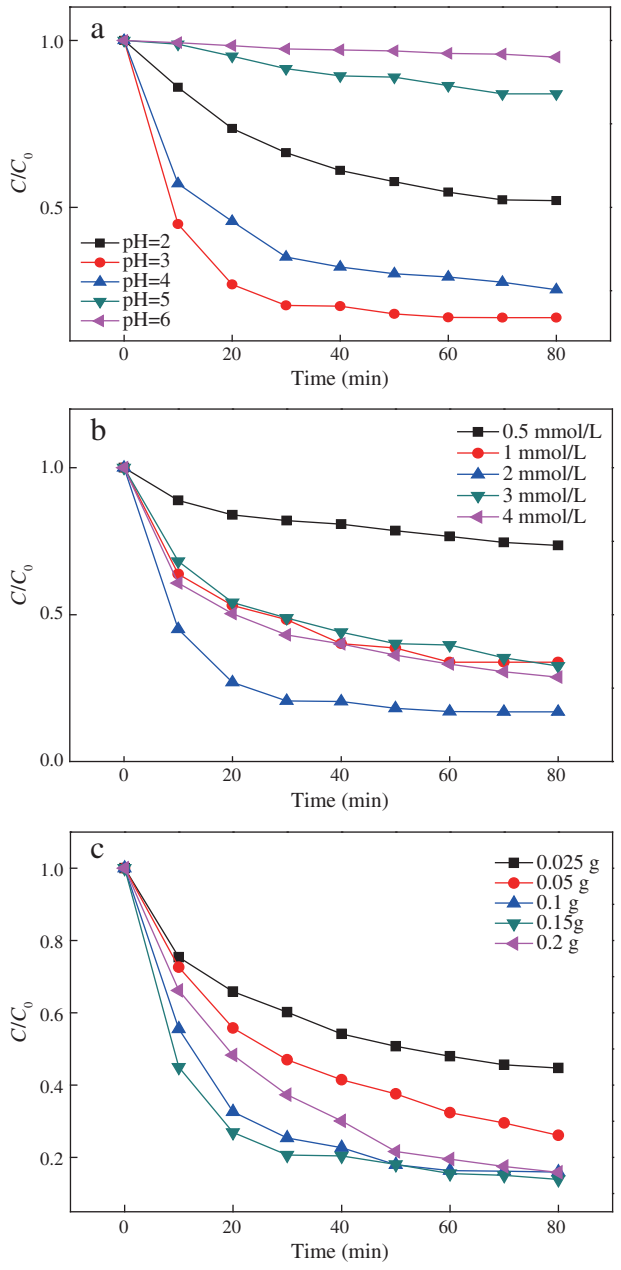

Fig. 6 – Effect of (a) initial pH, (b) initial concentration of oxalic acid and (c) catalyst dosage on photodegradation of OIII, C_{OII} 30 mg/L. Reaction conditions: (a) $W_{WPS\text{-}Fe\text{-}350}$ 0.1 g, 0.2 mmol/L $C_{oxalic\ acid}$, (b) $W_{WPS\text{-}Fe\text{-}350}$ 0.1 g, pH 3 and (c) $C_{oxalic\ acid}$ 2 mmol/L and pH 3.

2.4. Effect of oxalic acid concentration

As shown in Fig. 6b, a set of experiments were carried out at different oxalic acid initial concentrations in the range of 0.5–4.0 mmol/L. The results clearly indicated that the initial concentration of oxalic acid had a significant influence on the OII degradation ratio. In the low range (0.5–2.0 mmol/L), the OII degradation ratio increased significantly with the concentration of oxalic acid. However, excessive oxalic acid molecules present in the solution could adsorb on the Fe(III) sites on of the catalyst surface and competed with OII in reacting with the formed •OH radicals. Clearly, the optimal concentration of oxalic acid was 2 mmol/L in this photo-Fenton-like reaction system.

2.5. Effect of catalyst dosage

Since the reaction was carried out in a suspension of the heterogeneous catalyst (WPS-Fe-350), the catalyst content was an important factor, as it can influence the penetration of light into the suspension. Fig. 6c shows the dependence of OII photodegradation on the WPS-Fe-350 content. The OII photodegradation efficiency increased as the catalyst dosage increased from 0.025 to 0.15 g. More Fe(III)-oxalic acid species would be formed when more WPS-Fe-350 was added to the reaction solution, and as a result, more •OH would be generated. Nevertheless, further increasing WPS-Fe-350 dosage resulted in a slight decrease in the efficiency. The reaction suspension would become more turbid when excessive WPS-Fe-350 was added, which would reduce the penetration of light and decrease the formation of •OH. The optimal dosage of WPS-Fe-350 was 0.1 g, at which point the efficiency reached the maximal value of 86.4%.

2.6. Mechanism

Based on the results obtained above, WPS-Fe-350 exhibited efficient degradation ability toward OII in the presence of oxalic acid under UV-LED illumination. However, it was not clear whether the high degradation ratio of OII could be attributed to the presence of WPS-Fe-350 itself or to Fe ions in solution leaching from WPS-Fe-350 under acidic conditions. To clarify that this degradation reaction was not a homogenous one but rather a heterogeneous reaction, the concentration of iron ions present in the reaction solution was measured via ICP spectrometry when the reaction was complete. The results showed that the iron ion concentration of the solution was only 2.67 ppm, which was much lower than that of iron ion (12.2–40.2 ppm) in an iron oxide nanoparticle reaction system (Giraldi et al., 2009). After the reaction, 100 mL of the supernatant was collected by centrifugation. Subsequently, 5 mL of 630 mg/L OII was added

to the supernatant (100 mL) to form a 105 mL solution containing 30 mg/L OII for photodegradation. A comparison experiment was carried out using a 105 mL solution containing the same concentration of 30 mg/L OII and 0.1 g of WPS-Fe-350 under the same light source. As Fig. 7a shows, the degradation percentage of OII in the comparison experiment reached 90% at 80 min, while the degradation ratio of OII in the filtrate solution was only 22.6%. The result confirmed that photodegradation occurs not only on the surface of the catalyst but also in the bulk solution homogeneously, and the heterogeneous reaction predominates.

To ascertain the main mechanism by which OII was degraded during this photo-Fenton-like process, the degradation experiment was conducted in the presence of *tert*-butanol. The degradation process compared with normal conditions (without *tert*-butanol) is depicted in Fig. 7b. The results showed that the degradation percentage of OII decreased from 82.9% to 34.2% (47.8% reduction) in the presence of *tert*-butanol. As *tert*-butanol is traditionally employed as an efficient radical scavenger to determine the role of •OH in advanced oxidation processes (AOPs), it can be deduced that •OH plays a major role in the oxidative degradation of OII during the photo-Fenton-like process.

XPS investigation of WPS-Fe-350 was conducted before and after the degradation reaction (Fig. 8). XPS spectra indicated that the $Fe2P_{3/2}$ peak (curve A) broadens notably after the reaction, compared with that of WPS-Fe-350 before reaction (curve B). The full width at half maximum (FWHM) for WPS-Fe-350 before

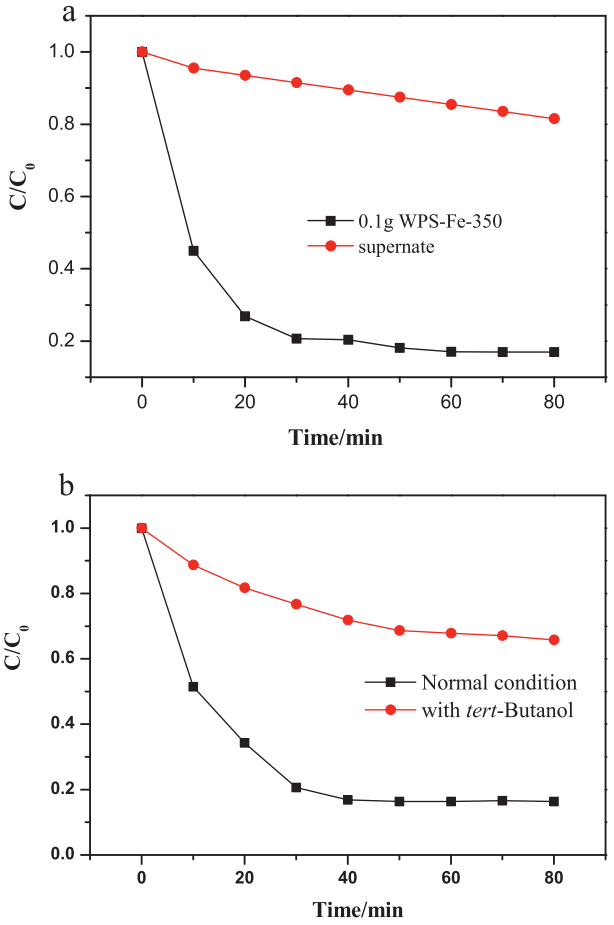

Fig. 7 – Effect of (a) homogenous and heterogeneous catalysis and (b) *tert*-Butanol on the degradation of OII.

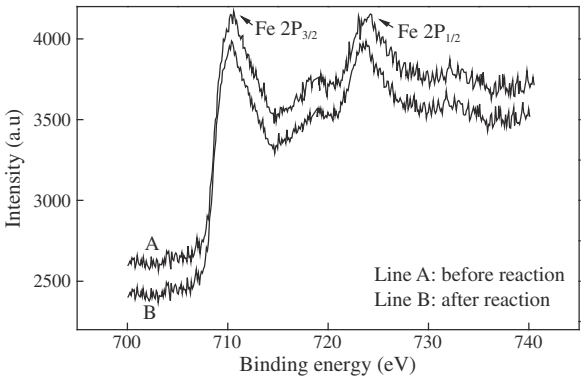

Fig. 8 – XPS spectra of iron in WPS-Fe-350 before and after reaction.

reaction was 3.57 eV while that for WPS-Fe-350 after reaction was 4.12 eV. The change of FWHM suggested that the molecular environment of the iron atoms on the surface of WPS-Fe-350 had been altered because the binding energy not only depends on the chemical state of the atoms, but also on their molecular environment. Based on the aforementioned result, it is further proved that the complex $[\equiv Fe^{III}(C_2O_4)_n]^{3-2n}$ was formed on the surface of WPS-Fe-350 during the photocatalytic process, because the formation constant is very large. Therefore, it is concluded that the formation of the photoactive complex $[\equiv Fe^{III}(C_2O_4)_n]^{3-2n}$ initiates the photocatalytic process.

Therefore, based on the previous reports (Balmer and Sulzberger, 1999; Zuo and Deng, 1997), we proposed a possible mechanism for WPS-Fe-350 as a heterogeneous catalyst for the photodegradation of OII, depicted by Eqs. (1)–(9). During this process, oxalic acid was first combined with Fe(III) on the surface of WPS-Fe-350 to form Fe(III)-oxalic acid complexes $[\equiv Fe^{III}(C_2O_4)_n]^{3-2n}$, which were able to be excited to generate a series of radicals, such as oxalate radicals $(C_2O_4)^{\bullet}$, carbon-centered radical $(CO_2)^{\bullet-}$, superoxide ion $(O_2^{\bullet-})$ and (hydroxyl radical) •OH, and form H_2O_2 in solution. Superoxide and hydroperoxyl radicals ($\bullet O_2^-/\bullet O_2H$) (Eqs. (2), (3), (4), (5) and (6)) are generated as the key intermediates. H_2O_2 is derived from $\bullet O_2^-/\bullet O_2H$, (Eqs. (7) and (8)) and participates in a classical Fenton reaction with Fe(II), to produce •OH (Eq. (9)):

$$Fe(III) + nH_2C_2O_4 \rightarrow [Fe(III)(C_2O_4)_n]^{(2n-3)-} \quad (1)$$

$$[Fe(III)(C_2O_4)_n]^{(2n-3)-} + h\nu \rightarrow [Fe(III)(C_2O_4)_n]^{2-} + \bullet(C_2O_4)^- \quad (2)$$

$$[Fe(III)(C_2O_4)_n]^{(3-2n)-} + h\nu \rightarrow [Fe(III)(C_2O_4)_{(n-1)}]^{(4-2n)} + \bullet(C_2O_4)^- \quad (3)$$

$$\bullet(C_2O_4)^- \rightarrow CO_2 + \bullet(C_2O_4)^- \quad (4)$$

$$\bullet(CO_2)^- + O_2 \rightarrow CO_2 + \bullet O_2^- \quad (5)$$

$$\bullet O_2^- + H^+ \rightarrow \bullet O_2H \quad (6)$$

$$\bullet O_2^- + Fe^{3+} \rightarrow Fe^{2+} + O_2 \quad (7)$$

$$\bullet O_2^-/\bullet O_2H + nH^+ + Fe^{2+} \rightarrow Fe^{3+} + H_2O_2 \quad (8)$$

$$Fe^{2+} + H_2O_2 \rightarrow Fe^{3+} + OH^- + \bullet OH. \quad (9)$$

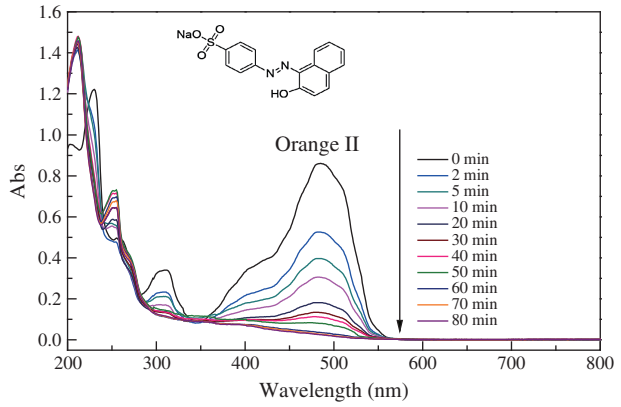

Fig. 9 – UV–Vis spectra of a typical degradation process. Initial conditions: C_{OII} 30 mg/L, $C_{oxalic\ acid}$ 2 mmol/L, pH 3.

Furthermore, in order to observe the molecular features and the structural transformation of OII during the degradation process, UV–Vis spectra changes of OII *vs.* time were observed (Fig. 9). At specified intervals during degradation, samples were analyzed by UV–Vis spectroscopy. As depicted, there were three major bands in the absorption spectrum of OII solution. A maximum absorption peak was observed at the visible region (485 nm) originating from the azo bond, the intensity of which reflected its concentration in the solution. This absorption peak decreased rapidly as the reaction proceeded, without the appearance of new absorption peaks. Additionally, the other two bands detected in the ultraviolet region (229 and 310 nm) were assigned to benzene-like structures in the OII molecule. As the reaction proceeded, the decrease of the absorbance at 229 nm as well as 310 nm was thought to be due to aromatic fragmentation in the OII molecule and its intermediates (Lau et al., 2014; Li et al., 2013).

2.7. *Reusability and stability*

Reuse experiments were carried out in order to test the catalytic activity of WPS-Fe-350 during the photodegradation OII process and to observe the reusability of the catalyst (Fig. 10). The catalyst was evaluated in five successive cycles

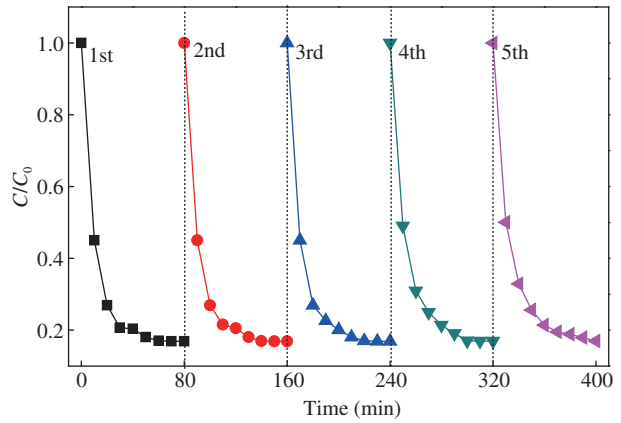

Fig. 10 – Cycling tests of WPS-Fe-350 for the degradation of OII. Initial conditions: C_{OII} 30 mg/L, $C_{oxalic\ acid}$ 2 mmol/L, pH = 3.

at optimal conditions (30 mg/L OII, 2.0 mmol/L oxalic acid at pH 3.0 and 0.1 g catalyst), and the reaction time was approximately 80 min for each cycle. After the completion of each run, the catalyst was separated and washed with deionized water several times. The degradation percentages of OII in all five cycles were more than 80.0%. The degradation was 83.2% at the first cycle and 82.3% at the fifth cycle. The results indicated the low cost and easily prepared catalyst (WPS-Fe-350) was reusable and has excellent potential for engineering application.

3. Conclusions

In the current work, a low-cost waste paper sludge-derived heterogeneous catalyst (WPS-Fe-350) was synthesized via a facile method and tested as heterogeneous catalyst for photodegradation of OII in aqueous solution. Since this process directly uses WPS-Fe-350 as heterogeneous catalyst and does not need the addition of H_2O_2, and exhibits high efficiency even under low energy consuming UV-LED, it is an economically viable way for degradation of dyes in wastewaters. Under optimum conditions (1 g/L of catalyst, 2 mmol/L of oxalic acid, 30 mg/L of MB), 86.4% degradation and 44.5% TOC removal were achieved within 80 min under UV-LED illumination. The photodegradation efficiency was significantly influenced by key factors such as catalyst dosage, initial concentration of oxalic acid and the initial pH. Furthermore, the as-synthesized catalyst exhibited negligible iron leaching and high catalytic activity after five reaction cycles. These results all demonstrate that WPS-Fe-350 is a promising catalyst, and this photo-Fenton like process is a potentially viable technique for degradation of dyes in real contaminated waters.

Acknowledgments

This work was supported by the Major Science and Technology Projects Focus on Social Development Projects of Zhejiang Province (Nos. 2014C03002 and 2012C03004-1).

REFERENCES

Balmer, M.E., Sulzberger, B., 1999. Atrazine degradation in irradiated iron/oxalate systems: effects of pH and oxalate. Environ. Sci. Technol. 33 (14), 2418–2424.

Calisto, V., Ferreira, C.I.A., Santos, S.M., Victoria Gil, M., Otero, M., Esteves, V.I., 2014. Production of adsorbents by pyrolysis of paper mill sludge and application on the removal of citalopram from water. Bioresour. Technol. 166, 335–344.

Chen, Q.K., Ji, F.Y., Liu, T.Y., Yan, P., Guan, W., Xu, X., 2013. Synergistic effect of bifunctional Co–TiO_2 catalyst on degradation of rhodamine B: Fenton-photo hybrid process. Chem. Eng. J. 229, 57–65.

Devi, P., Saroha, A.K., 2014. Synthesis of the magnetic biochar composites for use as an adsorbent for the removal of pentachlorophenol from the effluent. Bioresour. Technol. 169, 525–531.

Faust, B.C., Zepp, R.G., 1993. Photochemistry of aqueous iron(III)-polycarboxylate complexes: roles in the chemistry of atmospheric and surface waters. Environ. Sci. Technol. 27 (12), 2517–2522.

Fukuchi, S., Nishimoto, R., Fukushima, M., Zhu, Q.Q., 2014. Effects of reducing agents on the degradation of 2,4,6-tribromophenol in a heterogeneous Fenton-like system with an iron-loaded natural zeolite. Appl. Catal. B 147, 411–419.

Giraldi, T.R., Arruda, C.C., Da Costa, G.M., Longo, E., Ribeiro, C., 2009. Heterogeneous Fenton reactants: a study of the behavior of iron oxide nanoparticles obtained by the polymeric precursor method. J. Sol-Gel Sci. Technol. 52 (2), 299–303.

Guo, S., Zhang, G.K., Wang, J.Q., 2014. Photo-Fenton degradation of rhodamine B using Fe_2O_3–kaolin as heterogeneous catalyst: characterization, process optimization and mechanism. J. Colloid Interface Sci. 433, 1–8.

Guo, S., Zhang, G.K., Yu, J.C., 2015. Enhanced photo-Fenton degradation of rhodamine B using graphene oxide–amorphous $FePO_4$ as effective and stable heterogeneous catalyst. J. Colloid Interface Sci. 448, 460–466.

Haag, W.R., David Yao, C.C., 1992. Rate constants for reaction of hydroxyl radicals with several drinking water contaminants. Environ. Sci. Technol. 26 (5), 1005–1013.

Hamzeh, Y., Ashori, A., Mirzaei, B., 2011. Effects of waste paper sludge on the physico-mechanical properties of high density polyethylene/wood flour composites. J. Polym. Environ. 19 (1), 120–124.

Hossaini, H., Moussavi, G., Farrokhi, M., 2014. The investigation of the LED-activated *FeFNS*-TiO_2 nanocatalyst for photocatalytic degradation and mineralization of organophosphate pesticides in water. Water Res. 59, 130–144.

Karthikeyan, S., Judia Magthalin, C., Mandal, A.B., Sekaran, G., 2014. Controlled synthesis and characterization of electron rich iron(III) oxide doped nanoporous activated carbon for the catalytic oxidation of aqueous ortho phenylene diamine. RSC Adv. 4 (37), 19183–19195.

Karthikeyan, S., Titus, A., Gnanamani, A., Mandal, A.B., Sekaran, G., 2011. Treatment of textile wastewater by homogeneous and heterogeneous Fenton oxidation processes. Desalination 281, 438–445.

Kremer, M.L., 1999. Mechanism of the Fenton reaction. Evidence for a new intermediate. Phys. Chem. Chem. Phys. 1 (15), 3595–3605.

Lau, Y.Y., Wong, Y.S., Teng, T.T., Morad, N., Rafatullah, M., Ong, S.A., 2014. Coagulation-flocculation of azo dye acid orange 7 with green refined laterite soil. Chem. Eng. J. 246, 383–390.

Lei, J., Liu, C.S., Li, F.B., Li, X.M., Zhou, S.G., Liu, T.X., et al., 2006. Photodegradation of orange I in the heterogeneous iron oxide–oxalate complex system under UVA irradiation. J. Hazard. Mater. 137 (2), 1016–1024.

Li, F.B., Li, X.Z., Li, X.M., Liu, T.X., Dong, J., 2007. Heterogeneous photodegradation of bisphenol A with iron oxides and oxalate in aqueous solution. J. Colloid Interface Sci. 311 (2), 481–490.

Li, H.Y., Gong, Y.H., Huang, Q.Q., Zhang, H., 2013. Degradation of orange II by UV-assisted advanced fenton process: response surface approach, degradation pathway, and biodegradability. Ind. Eng. Chem. Res. 52 (44), 15560–15567.

Liu, S.Q., Feng, L.R., Xu, N., Chen, Z.G., Wang, X.M., 2012. Magnetic nickel ferrite as a heterogeneous photo-Fenton catalyst for the degradation of rhodamine B in the presence of oxalic acid. Chem. Eng. J. 203, 432–439.

Oller, I., Malato, S., Sánchez-Pérez, J.A., 2011. Combination of advanced oxidation processes and biological treatments for wastewater decontamination—a review. Sci. Total Environ. 409 (20), 4141–4166.

Pera-Titus, M., García-Molina, V., Baños, M.A., Giménez, J., Esplugas, S., 2004. Degradation of chlorophenols by means of advanced oxidation processes: a general review. Appl. Catal. B 47 (4), 219–256.

Shie, J.L., Lee, C.H., Chiou, C.S., Chang, C.T., Chang, C.C., Chang, C.Y., 2008. Photodegradation kinetics of formaldehyde using light sources of UVA, UVC and UVLED in the presence of composed silver titanium oxide photocatalyst. J. Hazard. Mater. 155 (1–2), 164–172.

Shu, H.Y., Chang, M.C., Chen, C.C., Chen, P.E., 2010. Using resin supported nano zero-valent iron particles for decoloration of Acid Blue 113 azo dye solution. J. Hazard. Mater. 184 (1–3), 499–505.

Siffert, C., Sulzberger, B., 1991. Light-induced dissolution of hematite in the presence of oxalate. A case study. Langmuir 7 (8), 1627–1634.

Wang, W., Liu, Y., Li, T.L., Zhou, M.H., 2014. Heterogeneous Fenton catalytic degradation of phenol based on controlled release of magnetic nanoparticles. Chem. Eng. J. 242, 1–9.

Wang, X.P., Lim, T.T., 2010. Solvothermal synthesis of C–N codoped TiO_2 and photocatalytic evaluation for bisphenol A degradation using a visible-light irradiated LED photoreactor. Appl. Catal. B 100 (1–2), 355–364.

Wei, S.Q., Liu, L., Li, H.B., Shi, J., Liu, Y., Shao, Z.C., 2012. Photodecolourization of orange II with iron corrosion products and oxalic acid in aqueous solution. Appl. Catal. A417-418, 253–258.

Yu, L.L., Achari, G., Langford, C.H., 2013. LED-based photocatalytic treatment of pesticides and chlorophenols. J. Environ. Eng. 139 (9), 1146–1151.

Yuan, S.J., Dai, X.H., 2014. Facile synthesis of sewage sludge-derived mesoporous material as an efficient and stable heterogeneous catalyst for photo-Fenton reaction. Appl. Catal. B154-155, 252–258.

Zuo, Y.G., Deng, Y.W., 1997. Iron(II)-catalyzed photochemical decomposition of oxalic acid and generation of H_2O_2 in atmospheric liquid phases. Chemosphere 35 (9), 2051–2058.